$BiVO_4$/3DOM TiO_2 nanocomposites: Effect of $BiVO_4$ as highly efficient visible light sensitizer for highly improved visible light photocatalytic activity in the degradation of dye pollutants

Meryam Zalfani,[a, b, c] Zhi-Yi Hu,[d, *] Wen-Bei Yu,[a] Mounira Mahdouani,[c] Ramzi Bourguiga,[c] Min Wu,[a, *] Yu Li,[a, *] Gustaaf Van Tendeloo,[d] Yahia Djoued[e] and Bao-Lian Su[a, b, f, *]

[a]State Key Laboratory of Advanced Technology for Materials Synthesis and Processing, Wuhan University of Technology, Luoshi Road 122, 430070, Wuhan, Hubei, China. E-mail: minwu@whut.edu.cn, yu.li@whut.edu.cn, baoliansu@whut.edu.cn

[b]Laboratory of Inorganic Materials Chemistry (CMI), University of Namur, 61 rue de Bruxelles, B-5000 Namur, Belgium. E-mail: bao-lian.su@unamur.be

[c]Laboratoire de Physique des Matériaux: Structure et Propriétés, Groupe Physique des Composants et Dispositifs Nanométriques, Faculté des Sciences de Bizerte, University of Carthage, 7021 Jarzouna-Bizerte, Tunisia

[d]EMAT (Electron Microscopy for Materials Science), University of Antwerp, Groenenborgerlaan 171, B-2020 Antwerp, Belgium. E-mail: zhiyi.hu@uantwerpen.be

[e]Université de Moncton, Campus de Shippagan, 218, boulevard J.-D. Gauthier, Moncton, Canada

[f]Clare Hall, University of Cambridge, Cambridge, United Kingdom. E-mail: bls26@cam.ac.uk

Abstract

A series of $BiVO_4$/3DOM TiO_2 nanocomposites have been synthesized and their photocatalytic activity was investigated under visible light irradiation using the RhB dye as model pollutant molecule in an aqueous solution. The effect of the amount of $BiVO_4$ as visible light sensitizer on the photocatalytic activity of $BiVO_4$/3DOM TiO_2 nanocomposites was highlighted. The heterostructured composite system leads to much higher photocatalytic efficiencies than bare 3DOM TiO_2 and $BiVO_4$ nanoparticles. As the proportion of $BiVO_4$ in $BiVO_4$/3DOM TiO_2 nanocomposites increases from 0.04 to 0.6, the photocatalytic performance of the $BiVO_4$/3DOM TiO_2 nanocomposites increases and then decreases after reaching a maximum at 0.2. This improvement in photocatalytic perfomance is related to 1) the interfacial electron transfer efficiency between the coupled materials, 2) the 3DOM TiO_2 inverse opal structure with interconnected pores providing an easy mass transfer of the reactant molecules and high accessibility to the active sites and large surface area and 3) the effect of light sensitizer of $BiVO_4$. Intensive studies on structural, textural, optical and surface properties reveal that the electronic interactions between $BiVO_4$ and TiO_2 lead to an improved charge separation of the coupled $BiVO_4$/TiO_2 system. The photogenerated charge carrier densities increase with increasing the $BiVO_4$ content, which acts as visible light sensitizer to the TiO_2 and is responsible for the enhancement in the rate of photocatalytic degradation. However, the photocatalytic activity is reduced when the $BiVO_4$ amount is much higher than that of 3DOM TiO_2. Two reasons could account for this behavior. First, with increasing $BiVO_4$ content, the photogenerated electron/hole pairs are accumulated at the surface of the $BiVO_4$ nanoparticles and the recombination rate increases as shown by the PL results. Second, decreasing the amount of 3DOM TiO_2 in the nanocomposite decreases the surface area as shown by the BET results. Moreover, the poor adsorptive properties of the $BiVO_4$ photocatalyst also affect the photocatalytic performance, in particular at higher $BiVO_4$ content. The present work demonstrates that $BiVO_4$/3DOM TiO_2 is a very promising heterojunction system for visible light photocatalytic applications.

1. Introduction

Semiconductor-based photocatalysis has attracted much attention as a potential solution for dealing with the global energy crisis and environmental pollution [1-4]. Among various types of semiconductors, TiO_2 has been the most suitable for widespread environmental applications due to its strong oxidizing ability. However, its photocatalytic activity under visible light irradiation needs to be enhanced [5-8]. Recently, considerable attention has been paid to the bismuth-based semiconductors [9-13]. Many Bi-based compounds possess a narrow band gap and exhibit high visible-light photocatalytic activity because of their hybridized O 2p and Bi 6s2 valence bands [14, 15]. Tremendous efforts have been devoted to the formation of a heterojunction between TiO_2 and narrow band gap semiconductors to enhance visible light responding photocatalyst with high activity. Monoclinic $BiVO_4$, having a band gap of ~2.4 eV, has been reported to possess excellent activity under visible irradiation [16-21]. Nevertheless, the rapid recombination rate of electron-hole pairs, the poor charge transport properties and the poor adsorptive behavior are still the main drawback of m-$BiVO_4$. The combination of TiO_2 and a sensitizer, $BiVO_4$, leading to the formation of an n heterojunction, can offer promising advantages in the photocatalytic system by improving visible absorption of TiO_2 and reducing the recombination rate of electron-hole of $BiVO_4$. With light irradiation, electrons and holes move in opposite direction under the driving of a built in electric-field. The charge carriers are thus separated and the carrier lifetime is prolonged [22, 23]. This charge separation prevents the electrons and holes from recombination. Thus, the electrons and holes have more opportunities to participate in reduction and oxidation reactions for the degradation of the organic dye on their surface. The formation of an interface between two semiconductors is an effective strategy in enhancing the separation of photogenerated electrons and holes and thus reducing the recombination rate. The well-matched energy band alignement is a key factor for the achievement of efficient heterojunctions [24, 25]. Recently the $BiVO_4/TiO_2$ heterojunction has been attracted considerable attention as a promising photocatalyst under visible light irradiation and has shown a significant suppression of the photogenerated electron-hole recombination [26-36]. Li et al. [34] showed that the photocatalytic performance of $BiVO_4/TiO_2$ heterojunction is drastically improved by controlling the contact facet owing to an especially high electron transfer capacity between TiO_2 and the {110} facet of $BiVO_4$. A suitable energy band alignment was found between both coupled semiconductors. An heterostructured m-$BiVO_4$/{001}-TiO_2 with shuriken-like shape was successfully synthesized by Zhu et al [35]

using a facile hydrothermal method. The obtained $BiVO_4/TiO_2$ heterojunction possessed a much higher photocatalytic activity for the degradation of methylene blue (MB) under visible light irradiation than the pure $BiVO_4$ and physically mixed $BiVO_4$-TiO_2 sample. This was attributed to a higher separation efficiency of the photogenerated electron-hole pairs under visible light irradiation. Xie et al. [32] fabricated $BiVO_4/TiO_2$ nanocomposites with different molar ratios and effective contacts by putting $BiVO_4$ nanoparticles into a TiO_2 sol, followed by a thermal treatment at 450°C. The photogenerated charge carriers in the $BiVO_4/TiO_2$ nanocomposite with a proper molar ratio of 5% displays a much longer lifetime and a higher separation efficiency than those in $BiVO_4$ alone. This can be attributed to the unusual spatial transfer of visible-excited high-energy electrons of $BiVO_4$ to TiO_2. Hu et al. [29] prepared $BiVO_4/TiO_2$ with a mass ratio of 1: 200 by a hydrothermal treatment for the benzene degradation reaction and claimed that their material was 3–4 times more active than nitrogen doped TiO_2 under visible light irradiation.

Zhang et al. [28] reported the synthesis of $BiVO_4/TiO_2$ by a one-step microwave hydrothermal method and found that the 20 wt% $TiO_2/BiVO_4$ nanocomposite exhibited better photocatalytic activity than pure monoclinic $BiVO_4$ and other percentages of TiO_2 in $BiVO_4$. This is because of its high crystallinity, narrow bandgap, and most importantly, the hierarchical heterostructure which can effectively separate photoinduced electron–hole pairs on the surface of $BiVO_4/TiO_2$ photocatalysts. $BiVO_4$/3DOM TiO_2 nanocomposites were synthesized for the first time via a hydrothermal method [36]. The results showed that 3DOM $BiVO_4/TiO_2$ nanocomposites possess a highly prolonged lifetime and an increased separation efficiency of visible light generated charges and an extraordinarily high photocatalytic activity. Owing to the intimate contact between $BiVO_4$ and large surface area 3DOM TiO_2, the photogenerated high energy charges can be easily transferred from $BiVO_4$ to the 3DOM TiO_2 support under the internal field induced by the different electronic band structures of the coupled semiconductors. It was also found that the larger the amount of $BiVO_4$ in the nanocomposite, the longer the duration of photogenerated charge separation and the higher the photocatalytic activity. 3DOM structures with an open interconnected porous network can also facilitate the diffusion of molecules and offer a larger surface area which is essential for the accessibility of the dye molecules to the photocatalysts and for a better dispersion of the $BiVO_4$ nanoparticles [37-41]. Therefore $BiVO_4$/3DOM TiO_2 nanocomposites show an enhanced photocatalytic efficiency compared with pure 3DOM TiO_2, dumbbell-like $BiVO_4$ nanoparticles, physically mixed $BiVO_4$ nanoparticles and 3DOM TiO_2 and $BiVO_4/TiO_2$

nanocomposites without a 3DOM structure. Although the combination of $BiVO_4$ nanoparticles and 3DOM TiO_2 is quite beneficial for photocatalytic activity, it is found that the amount of $BiVO_4$ affects significantly the recombination of photogenerated electron-holes, the visible light sensitizing efficiency, electron transfer from the $BiVO_4$ to TiO_2 and thus finally the photocatalytic activity. It is crucial to know how the amount of $BiVO_4$ will influence the formation of the heterojunction between $BiVO_4$ nanoparticles and 3DOM TiO_2. Since the photocatalytic reactions occur at the side of TiO_2 (conduction and valence band of TiO_2), it is important to know how a decreasing TiO_2 amount and an increasing $BiVO_4$ amount will modify the photocatalytic efficiency of $BiVO_4$/3DOM TiO_2 nanocomposites to design photocatalyts with best performance. Photocatalytic efficiency of the $BiVO_4$/TiO_2 system was evaluated in terms of degradation of organic pollaunts such as Rhodamine B (RhB) aqueous solution. Rhodamine B, a xanthene dye is widely used as a colorant in textiles and food stuffs, and is also a well-known water tracer fluorescent [42]. It is harmful to human beings and animals, and causes irritation of the skin, eyes and respiratory tract. The carcinogenicity, reproductive and developmental toxicity, neurotoxicity and chronic toxicity toward humans and animals have been experimentally proven [43, 44]. During the photocatalytic process, the dye molecules are adsorbed on the surface of the catalysts, where chemical bonds are broken and small organic molecules are released as decomposed products. When the photocatalyst is irradiated in the presence of water hydroxyl radicals $OH^{\bullet}$, as strong oxidant agent, are photogenerated. These reactive species are able to achieve a complete mineralization of organic dyes. Rhodamine B (RhB) is a common dye in the triphenylmethane family, which contains four N-ethyl groups ateither side of the xanthene ring. It has been reported that in the visible-light induced photocatalytic degradation of RhB, as N-ethyl-containing dye, three main steps, namely N-deethylation, cleavageof chromoporme and mineralization of dye, were frequently witnessed [45–47]. At the end of photocatalytic process, the RhB dye is completely mineralized into CO_2, H_2O [48–53].

In this work, a series of $BiVO_4$/3DOM TiO_2 nanocomposites with different compositions have been synthesized. The effect of $BiVO_4$ as visible light sensitizer on the photocatalytic activity has been studied. The $BiVO_4$ content in $BiVO_4$/3DOM TiO_2 nanocomposites has been optimized. The charge transfer and interaction between $BiVO_4$ with 3DOM TiO_2 have been discussed on the basis of structural, textural, optical and surface characterization. The present contribution will shed some light on the design of optimized photocatalys for dye pollutant aqueous removal.

2. Experimental

2.1 Synthesis of $BiVO_4$/3DOM TiO_2 nanocomposites

The fabrication of $BiVO_4$/3DOM TiO_2 nanocomposites was achieved via a hydrothermal strategy, as reported in our previous work [36] in which stoichiometric amounts of $Bi(NO_3)_3.5H_2O$ (Carl Roth, $98%, p.a. ACS) and NH_4VO_3 (Carl Roth, $98%, p.a.) were dissolved in a stoichiometric volume of an ethylene glycol–water mixture and stirred for about 10 min until a clear solution was formed. Then, the desired amount of 3DOM TiO_2 was added into the solution and sonicated for 15 min. After 1 h stirring, the obtained yellow coloured mixture was transferred into a Teflon-sealed autoclave which was maintained at 160°C for 24 h. The solid powders were recovered by centrifugation and washed three times with distilled water and absolute ethanol. Finally, the obtained solid was vacuum-dried at 60°C for 6 h and then calcined at 300°C for 1 h. Dumbbell-like $BiVO_4$ and 3DOM TiO_2 were taken as reference to evaluate the photocatalytic activity of both samples 0.04$BiVO_4$/3DOM TiO_2 and 0.08$BiVO_4$/3DOM TiO_2, the 0.04 and 0.08 designed the molar ratio Bi :Ti; the synthesized method was detailed in [36]. Herein, three nanocomposites were synthesized with different ratios labeled 0.2$BiVO_4$/3DOM TiO_2 0.4$BiVO_4$/3DOM TiO_2 and 0.6$BiVO_4$/3DOM TiO_2, respectively.

2.2 Materials characterization

The crystalline structure of the powder samples was characterized by powder X-ray diffraction (XRD) (a PANalytical X'pert Pro with Cu Ka radiation). The morphological properties were analyzed by scanning electron microscopy (SEM) (Jeol JSM-7500F). Part of transmission electron microscopy (TEM) study was performed on a Philips FEI-Tecnai 10 electron microscope with an accelerating voltage of 80 kV. Transmission electron microscopy (TEM), scanning transmission electron microscopy (STEM), and energy dispersive X-ray spectroscopy (EDX) were peformed on a FEI Osiris electron microscope fitted with Super-X windowless EDX dectector system, operated at 200kV. X-ray photoelectron spectroscopy (XPS) analysis was performed on a K-Alpha™ + X-ray photoelectron spectrometer (XPS). The binding energy for the C (1s) peak at 284.9 eV (relative to adventitious carbon from the XPS instrument itself) was used as a reference. Textural properties of the materials were evaluated via adsorption–desorption of nitrogen at -196 °C using a Micromeritics Tristar 3000

with prior outgassing. The UV-vis absorbance spectra were obtained using a UV-vis spectrophotometer (Perkin Elmer Lambda 35 UV-visible spectrometer fitted with a Labsphere for analysis in diffuse reflectance mode) in the range of 200–750 nm. Photoluminescence properties of the samples were studied by Perkin Elmer LS45 luminescence spectrometry. The photocatalyst podwer has been charged in smple holder supplied by spectrometry manufacturer and then photoluminescence was then recorded.

2.3 Photocatalytic testing

Photocatalytic performances of the as-prepared photocatalysts were measured under visible light irradiation (400–800 nm) using 6 neon lamps of 18 W. The luminous power of each lamp was 1250 lm and the total luminouspower was 7500 lm in the photocatalytic reactor. The reaction temperature was maintained at room temperature. We use a very strong ventilation system and the temperature of the photocatalytic reactor is followed to ensure the room temperature of photocatalytic reactor. In each experiment 20 mg of the photocatalyst was placed in 50 mL of a reactant solution with an initial concentration of 10^{-3} M of RhB. The suspension was poured into a quartz tube, inserted into a reactor and stirred in the dark for 120 min to ensure adsorption/desorption equilibrium prior to irradiation. During irradiation, 2 mL of the suspension was removed at a given time interval for subsequent RhB concentration analysis.

3. Results and discussions

3.1 Phase composition

XRD patterns of the as-prepared $BiVO_4$/3DOM TiO_2 nanocomposites with different $BiVO_4$ content are illustrated in Fig. 1, and compared with those of dumbbell-like $BiVO_4$ nanoparticles and 3DOM TiO_2 with an inverse opal structure. The $BiVO_4$ particles (Fig. 1g) exhibit distinctive diffraction peaks, which can be well indexed to monoclinic $BiVO_4$ (JCPDS card No. 14-0688). For pure 3DOM TiO_2 particles (Fig.1a), the diffraction peaks are assigned to the anatase phase, matching very well with JCPDS card No. 21-1272. The diffraction peaks of the 0.04$BiVO_4$/3DOM TiO_2 (Fig. 1b), 0.08$BiVO_4$/3DOM TiO_2 (Fig. 1c), 0.2$BiVO_4$/3DOM TiO_2 (Fig. 1d), 0.4$BiVO_4$/3DOM TiO_2 (Fig. 1e) and 0.6$BiVO_4$/3DOM TiO_2 (Fig. 1f) nanocomposite photocatalysts, are composed of the characteristic peaks corresponding to monoclinic $BiVO_4$ and anatase TiO_2. For all $BiVO_4$-TiO_2 heterojunction samples the introduction of $BiVO_4$ nanoparticles did not change the crystal phase and crystallinity of TiO_2.

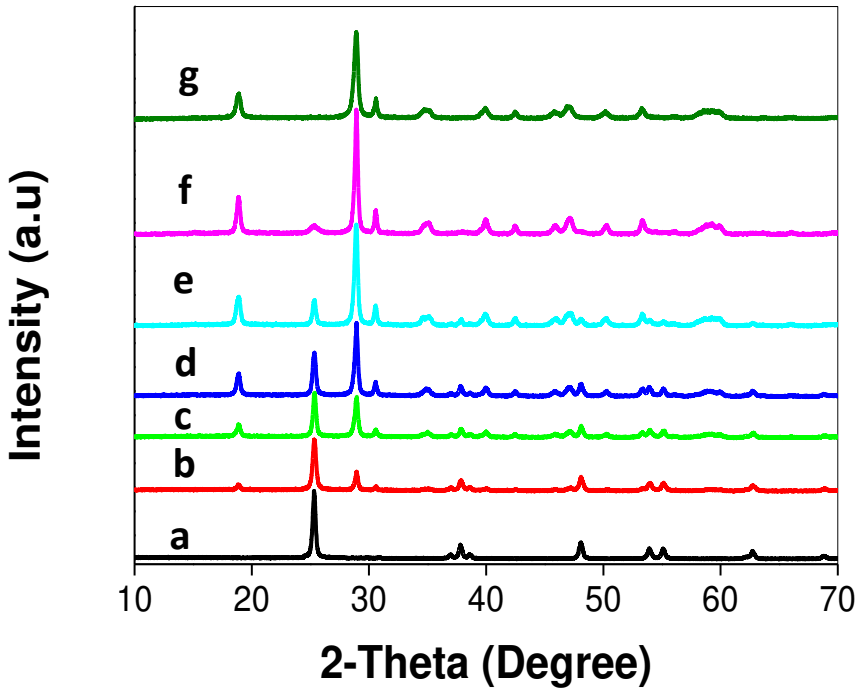

Fig. 1. XRD patterns of 3DOM TiO_2 (a), $BiVO_4$/3DOM TiO_2 nanocomposites with different mole ratios:(b) 0.04 $BiVO_4$/3DOM TiO_2, (c) 0.08$BiVO_4$/3DOM TiO_2, (d) 0.2$BiVO_4$/3DOM TiO_2, (e) 0.4$BiVO_4$/3DOM TiO_2 and (f) 0.6$BiVO_4$/3DOM TiO_2 and $BiVO_4$ nanoparticles (g).

3.2 Morphology

Fig. 2 shows SEM images of the 0.2 $BiVO_4$/3DOM TiO_2 compound at different magnification. As can be seen the 0.2 $BiVO_4$/3DOM TiO_2 nanocomposite exhibits a dual morphology, spherical-like nanoparticles corresponding to $BiVO_4$, incorporated in the large macropores of 3DOM TiO_2. As for the $BiVO_4$ nanoparticles, the average diameter is ranging from 70 - 90 nm. The TiO_2 support exhibits a high quality 3DOM inverse opal structure. The underlying layer of pores and porous walls can be clearly observed, indicating that the sample possesses a three-dimensionally well-open, ordered and interconnected macroporous network.

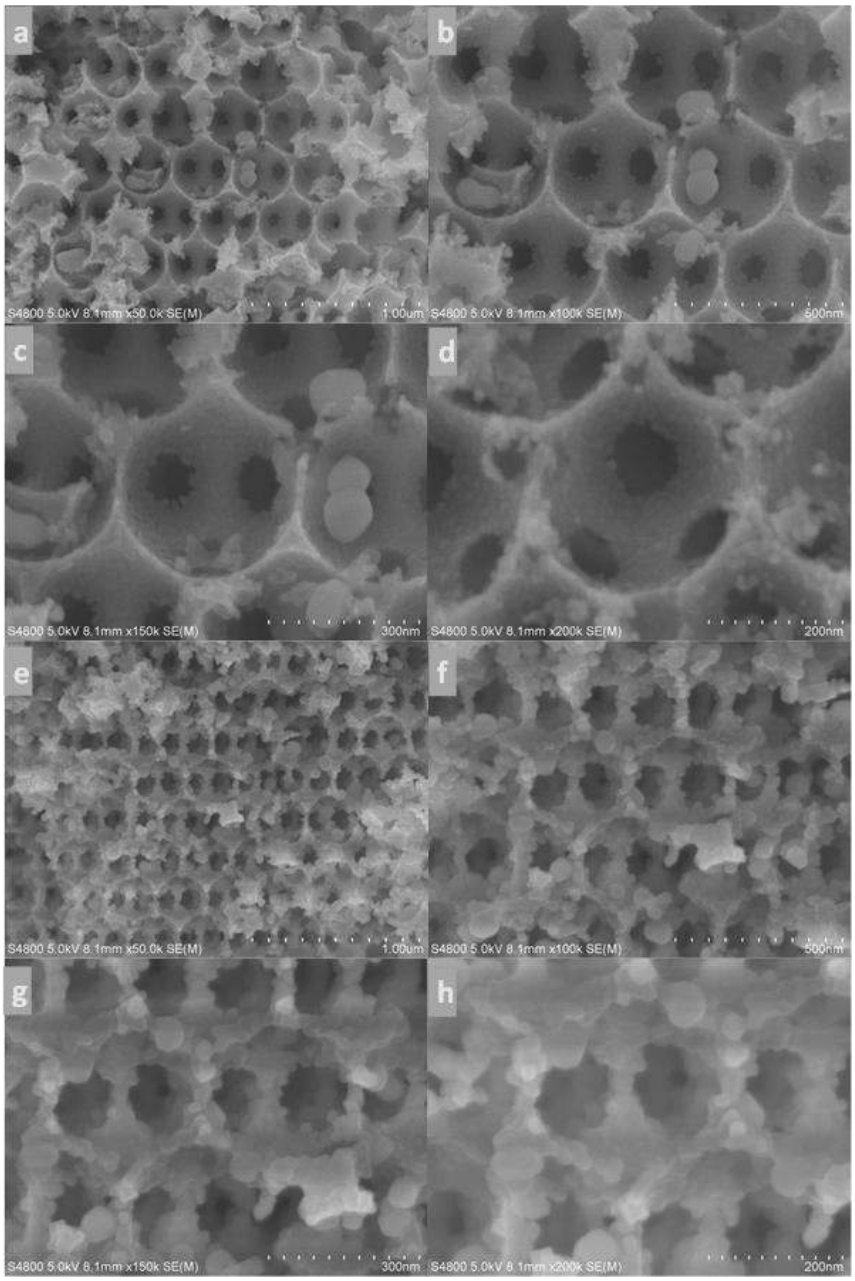

Fig. 2. SEM images of 0.2$BiVO_4$/3DOM TiO_2 nanocomposite.

Transmission electron microscopy (TEM) has been used to prove the formation of heterojunctions in the $BiVO_4$/3DOM TiO_2 nanocomposite. The low magnification TEM images of the 0.2BVO_4/3DOM TiO_2 photocatalyst in Fig. 3a confirm the existence of two morphologies: spherical-like $BiVO_4$ nanoparticles embedded in the 3DOM TiO_2 support with an interconnected porous structure (Fig. 3b). As can be clearly seen from Fig. 3c, the TiO_2 is present as small nanoparticles. The corresponding HRTEM image (Fig. 3d) exhibits two kinds of lattice fringes, one of d=0.352 nm which matches the (101) crystallographic planes of anatase TiO_2, the second of d=0.312 nm which corresponds to the (130) crystallographic plane of monoclinic $BiVO_4$. It is clear that a heterojunction structure with intimate contact at a nano scale is formed between both semiconductors.

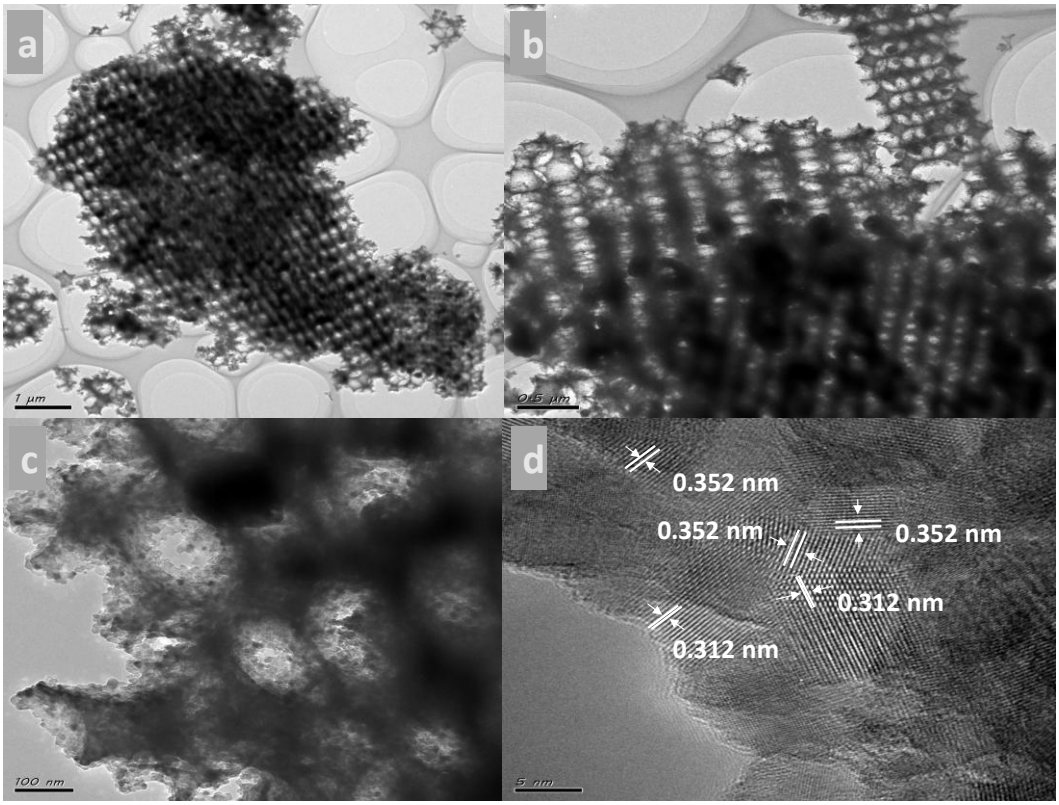

Fig. 3. TEM images (a-c) and HRTEM image (d) of the 0.2$BiVO_4$ /3DOM TiO_2 nanocomposite.

The Z-contrast HAADF-STEM image in Fig. 4a reveals the highly ordered 3DOM TiO_2 inverse opal structure with the embedded spherical $BiVO_4$ particles more clearly because the

image intensity is approximately proportional to the square of the atomic number (Z^2) and the thickness of the specimen. The higher magnification HAADF-STEM image (Fig. 4b) shows the dispersion of the $BiVO_4$ nanoparticles of 70-90 nm (in good agreement with the SEM image in Fig. 2). The corresponding EDX elemental maps (Fig 4c, d and e) show very clearly the highly homogeneous dispersion of the $BiVO_4$ nanoparticles. The enlarged

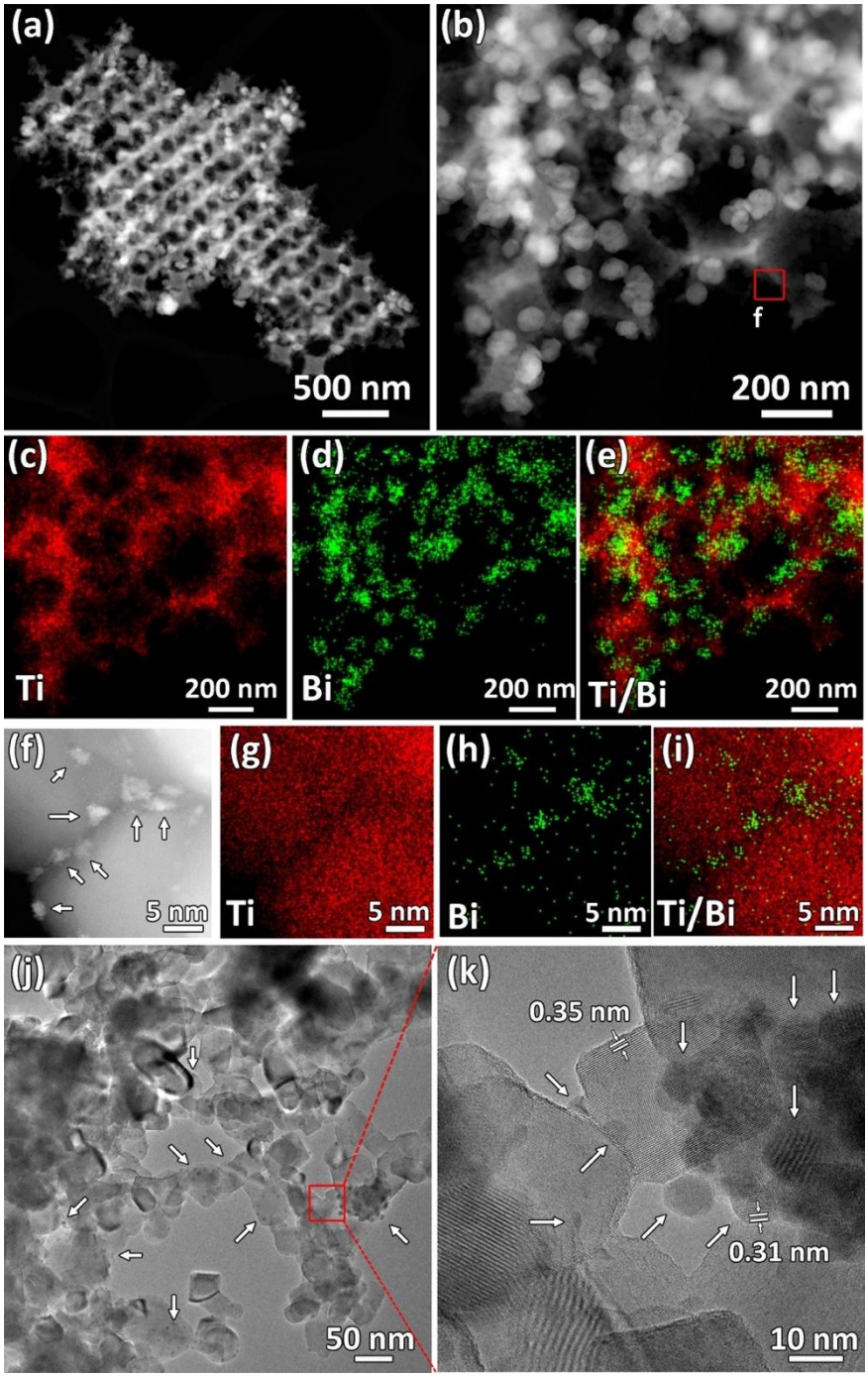

Fig. 4. (a, b, f) HAADF-STEM images at different magnification, (c-e) corresponding EDX elemental maps of the whole area of (b). (g-i) corresponding EDX elemental maps of the

whole area of (f), (i) TEM image, (k) HRTEM image of the area indicated in (j) with a red box. The $BiVO_4$ nanoparticles are indicated by white arrows.

HAADF-STEM image (Fig. 4f) of a small zone (Fig. 4b) and its corresponding EDX elemental maps (Fig. 4g, h and i) indicate the existence of very small nanoparticles of around 2-5 nm of $BiVO_4$ imbeded in the framework of the 3DOM TiO_2 structure. The HRTEM of the corresponding zone (Fig. 4k) confirms that $BiVO_4$ nanoparticles are in direct and intimate contact with the TiO_2 nanoparticles.

3.3 XPS analysis

The X-ray photoelectron spectroscopy (XPS) was carried out to further determinate the chemical states and the composition of the $BiVO_4$/3DOM TiO_2 nanocomposites. For the sake of the clarity, only the results of 0.2$BiVO_4$/3DOM TiO_2 are presented and analyzed and compared with pure 3DOM TiO_2 and pure $BiVO_4$ nanoparticle photocatalysts. From Fig. 5, four dominate elements (Bi, V, Ti, and O) are found, confirming the presence of $BiVO_4$ and TiO_2 in the sample. Fig. 5a shows the Bi 4f spectra of the 0.2 $BiVO_4$/TiO_2 sample compared with that of $BiVO_4$. There are two strong peaks at 159 eV and 164.4 eV, which are assigned to Bi 4f7/2 and Bi 4f5/2 and correspond to Bi^{3+} [10, 54]. Compared with pure $BiVO_4$ nanoparticles there is a shift of 0.4 eV in the position of Bi 4f7/2 (164 eV) and Bi 4f5/2 (158.6). Two symmetric spectra of V 2p1/2 and V 2p3/2 in the 0.2$BiVO_4$/3DOM TiO_2 composite at binding energies of 524.5 and 516.8 eV, respectively (shown in Fig. 5b) are characteristic of V^{5+} ions [55]. Compared with pure $BiVO_4$, a shift of 0.5 eV is observed in the peak position corresponding to V 2p (524.0 for the V 2p1/2 orbit and 516.3 eV for V 2p3/2). In Fig. 5d, the 0.2$BiVO_4$/3DOM TiO_2 composite presents two spectra of Ti 2p at 458.1 and 463.8 eV assigned to Ti 2p3/2 and Ti 2p1/2, respectively. The spectrum separation between Ti 2p3/2 and Ti 2p1/2 is 5.7 eV, which stems from the expected oxidation state of Ti^{4+} [56, 57]. A shift of 0.7 eV in the peak position of Ti 2p in the 0.2$BiVO_4$/3DOM TiO_2 compared with pure TiO_2 (458.8 eV and 464.5 eV) indicates that a charge transfer between TiO_2 and $BiVO_4$ occurred after the formation of the nanocomposite. The O 1s spectrum is located at 529.1 eV with an asymmetric pattern as shown in Fig. 5e. The primary spectrum indicates the presence of O^{2-} ions, while the additional shoulders at higher energies are assigned to surface OH^- groups and/or chemisorbed H_2O [58]. For the $BiVO_4$ and TiO_2 samples, the O1s peaks are located at 529.4 and 530 eV, respectively. As we can note, the Bi 4f, V 2p, Ti 2p and O 1s peaks in the 0.2$BiVO_4$/3DOM TiO_2 show a significant shift

confirming that a significant interaction exists between the two coupled semiconductors. As for the 0.08$BiVO_4$/3DOM TiO_2 nanocomposite, as detailed in [36] the shift values of the Bi4f, V2p, Ti2p and O1s elements were found to be: 0.3, 0.3, 0.6 and 0.2, respectively.

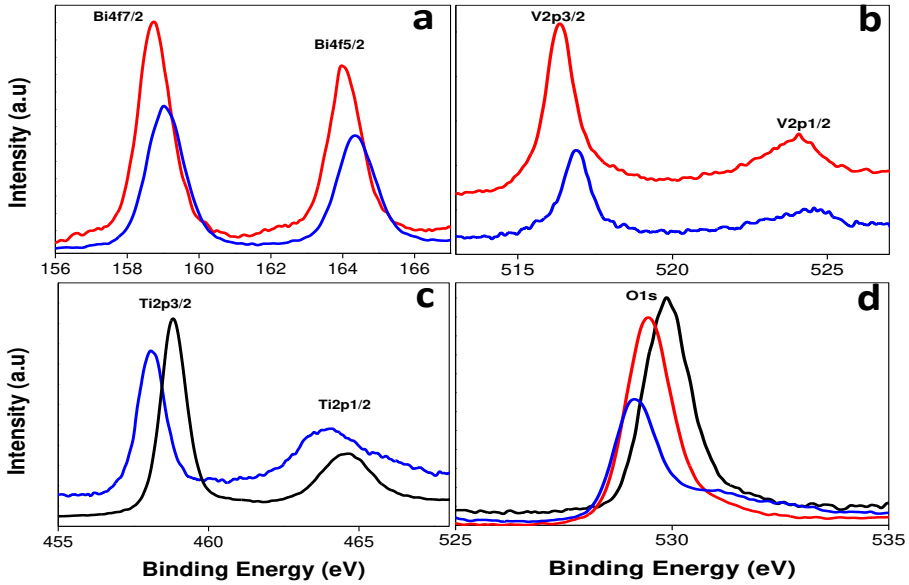

Fig. 5. XPS spectra of (a) Bi4f, (b) V2p, (c) Ti2p and (d) O1s for 0.2$BiVO_4$/3DOM TiO_2 (blue line) compared with pure $BiVO_4$ nanoparticles (red line) and 3DOM TiO_2 inverse opal structure (black line).

3.4 Textural properties

The N_2 adsorption–desorption isotherms and pore-size distributions curves of the samples are illustrated in Fig. 5. The obvious macroporous structure enables each of the 3DOM TiO_2, 0.2$BiVO_4$/3DOM TiO_2, 0.4 $BiVO_4$/3DOM TiO_2 and 0.6 $BiVO_4$/3DOM TiO_2 samples to exhibit a type II isotherm, according to IUPAC classification, with a type H3 hysteresis loop in the relative pressure range of 0.9–1.0. BET specific surface areas of pure $BiVO_4$ nanoparticles, 3DOM TiO_2 inverse opal structure and $BiVO_4$/3DOM TiO_2 nanocomposites with different molar ratios are shown in Table1.

The 3DOM TiO_2 sample shows a higher surface area than the composite samples with a value of 30 m^2/g. It should be noted that large surface areas of the photocatalysts play an important role in enhancing photocatalytic activities by favoring the adsorption of small dye molecules at the active surface of these samples. However, it decreases significantly after the introduction of $BiVO_4$ nanoparticles to about 15 m^2/g for 0.2$BiVO_4$/3DOM TiO_2, 12 m^2/g for

0.4$BiVO_4$/3DOM TiO_2 and 7 m^2/g for 0.6$BiVO_4$/3DOM TiO_2. The BET surface for 0.04$BiVO_4$/3DOM TiO_2 and 0.08$BiVO_4$/3DOM TiO_2 nanocomposites and $BiVO_4$ nanoparticles is found to be 25, 17 and 4 m^2/g, respectively [46]. Moreover, the pore-size distribution calculated by the desorption branch of isotherm for all samples, as shown by the inset curves in Fig. 6, shows a narrow pore-size distribution ranging from 2.3 to 9 nm, due to aggregations of the nanoparticles. The calculated BET for all samples are summarized in Fig. 7 and it is confirms that there is a significant decrease when increasing the amount of $BiVO_4$ nanoparticles.

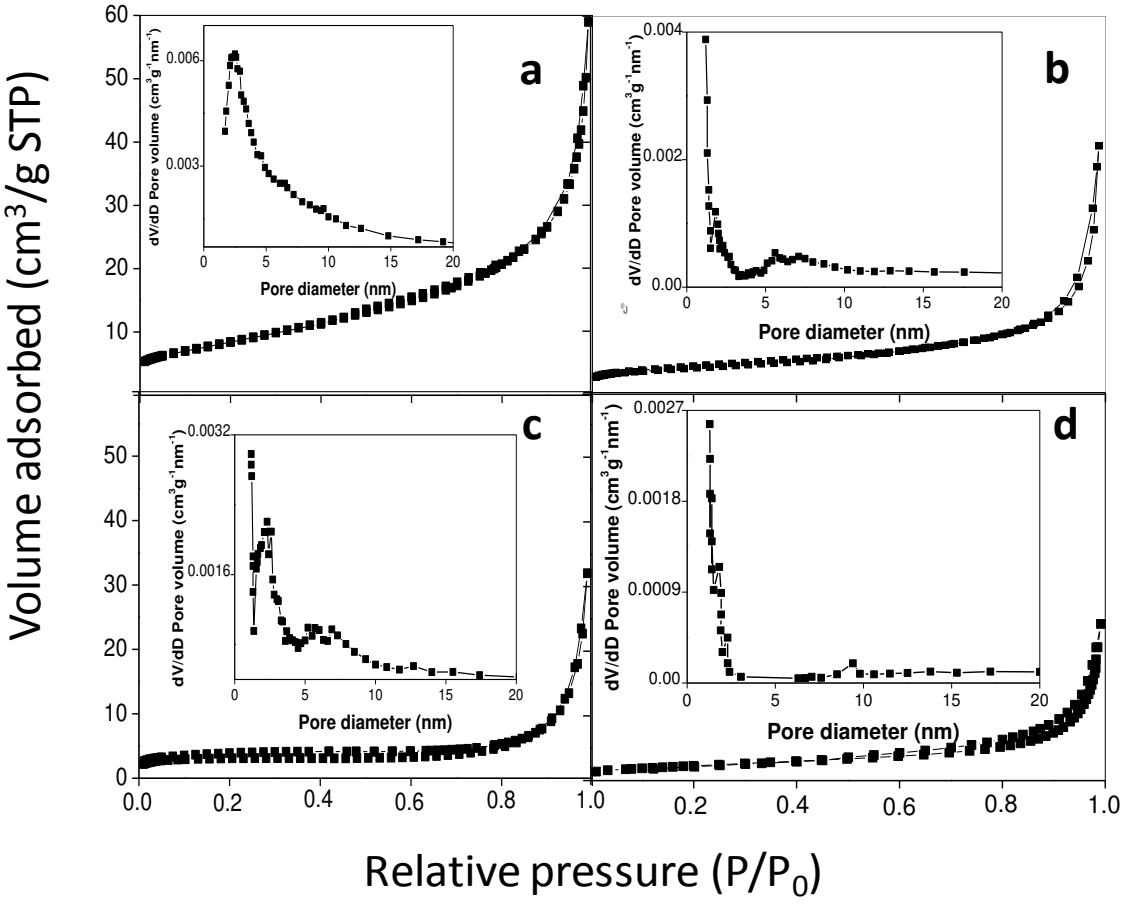

Fig. 6. Nitrogen adsorption-desorption isotherms and pore size distribution curve (inset) of (a) 3DOM TiO_2, (b) 0.2$BiVO_4$/3DOM TiO_2, (c) 0.4$BiVO_4$/3DOM TiO_2 and (d) 0.6$BiVO_4$/3DOM TiO_2 nanocomposites photocatalysts.

Table 1 BET specific surface area, average pore diameter and pore volume of 3DOM TiO_2, $BiVO_4$ nanoparticles and $BiVO_4$/3DOM TiO_2 heterojunction photocatalysts

Materials	S_{BET} (m^2g^{-1})	Pore size (nm)	Pore volume (cm^3g^{-1})
3DOM TiO_2	30	2.3	0.0062
0.04$BiVO_4$/3DOM TiO_2	25	2.4, 8	0.0028
0.08$BiVO_4$/3DOM TiO_2	17	2.5, 7	0.0022
0.2$BiVO_4$/3DOM TiO_2	15	2.1, 5	0.004
0.4$BiVO_4$/3DOM TiO_2	11	2.2, 6	0.0032
0.6$BiVO_4$/3DOM TiO_2	7	2.3, 9	0.0027
$BiVO_4$	4	23	0.00032

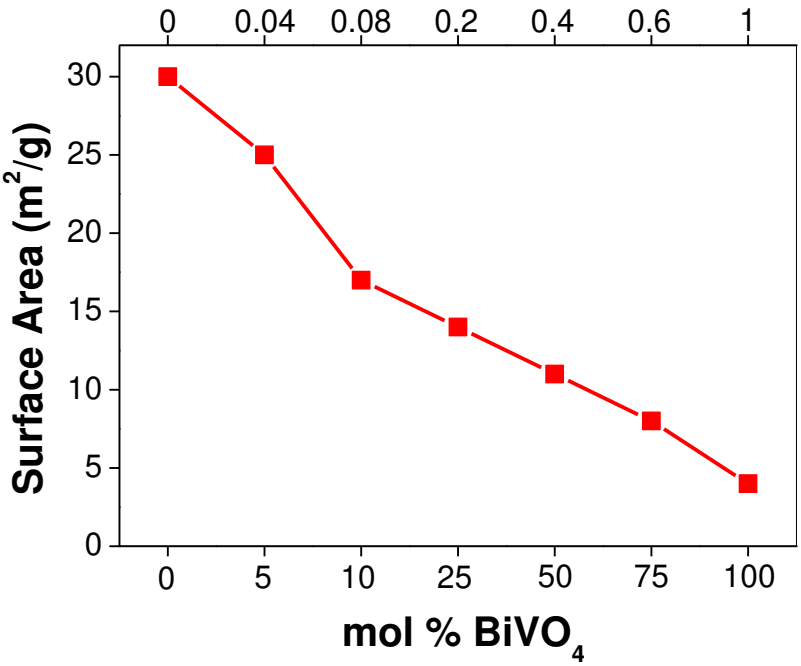

Fig. 7. BET surface area variation with increasing molar ratios.

3.5 Optical properties

The optical absorption property of the semiconductor is a key factor in affecting the photocatalytic performance [59]. Fig. 8 shows the UV-vis absorption spectra of the as-prepared samples. The pure 3DOM TiO_2 (spectrum a) exhibits photoresponsiveness in the UV region (wavelength below 395 nm) because of its wide energy band gap (3.2 eV). In addition, the absorption edge of $BiVO_4$ nanoparticles (spectrum e), estimated at 525nm, is assigned to the band transition from the Bi 6s orbital to a V 3d conduction band. As can be clearly seen, the absorption in the visible light range of $BiVO_4$/3DOM TiO_2 samples remarkably increases with the increase of $BiVO_4$ nanoparticles. The absorption edge of the 0.2$BiVO_4$/3DOM TiO_2, 0.4$BiVO_4$/3DOM TiO_2 and 0.6$BiVO_4$/3DOM TiO_2 nanocomposites (spectra b-d) are quite close to that of $BiVO_4$ nanoparticles and their absorption intensities were obviously higher than that of 3DOM TiO_2. Compared with 0.04$BiVO_4$/3DOM TiO_2 and 0.08$BiVO_4$/3DOM TiO_2 nanocomposites, as shown in [36], the absorption edge is more shifted to the visible range with increasing the $BiVO_4$ amount in the nanocomposite.

Moreover, the energy band structures of a semiconductor stay important in determining its photocatalytic activity. The relation between the absorbance and incident photon energy $h\nu$ can be described by the following equation:

$$(\alpha h\nu) = A\,(h\nu - Eg)^{1/2}$$

where α, Eg, h, ν and A represent the absorption coefficient, the band-gap energy, the Planck constant, the incident light frequency and a constant, respectively. The band-gap energy can therefore be estimated from the intercept of the plots of $(\alpha h\nu)^{1/2}$ versus $(h\nu)$ as illustrated in Fig. 7(b). The corresponding band gap energies are found to be 2.38, 3.14, 2.39, 2.4 and 2.43 eV for $BiVO_4$ nanoparticles, 3DOM TiO_2 inverse opal structure, 0.2 $BiVO_4$/3DOM TiO_2, 0.4 $BiVO_4$/3DOM TiO_2 and 0.6 $BiVO_4$/3DOM TiO_2 nanocomposites, respectively. The estimated band gap energies of 0.04 $BiVO_4$/3DOM TiO_2 and 0.08 $BiVO_4$/3DOM TiO_2 photocatalysts were found to be 2.44 and 2.41 eV.

The photoluminescence (PL) is a facile technique to study the photochemical properties of semiconductor materials, where the PL emission mainly originates from the recombination of the excited electrons and holes [60]. Fig. 9 presents the PL spectra of the 3DOM TiO_2 and $BiVO_4$/3DOM TiO_2 samples. The pure TiO_2 inverse opal structure (spectrum a) gives a strong PL signal located at 420 nm mainly resulting from band edge free excitons and four obvious PL peaks at about 442, 457, 485 and 527 nm, respectively, possibly resulting from binding excitons [61, 62]. It has been reported that a higher peak intensity

indicates a larger probability of charge carrier recombination [63]. Semiconductors with lower PL intensities usually exhibit higher photocatalytic activity due to a lower charge recombination rate.

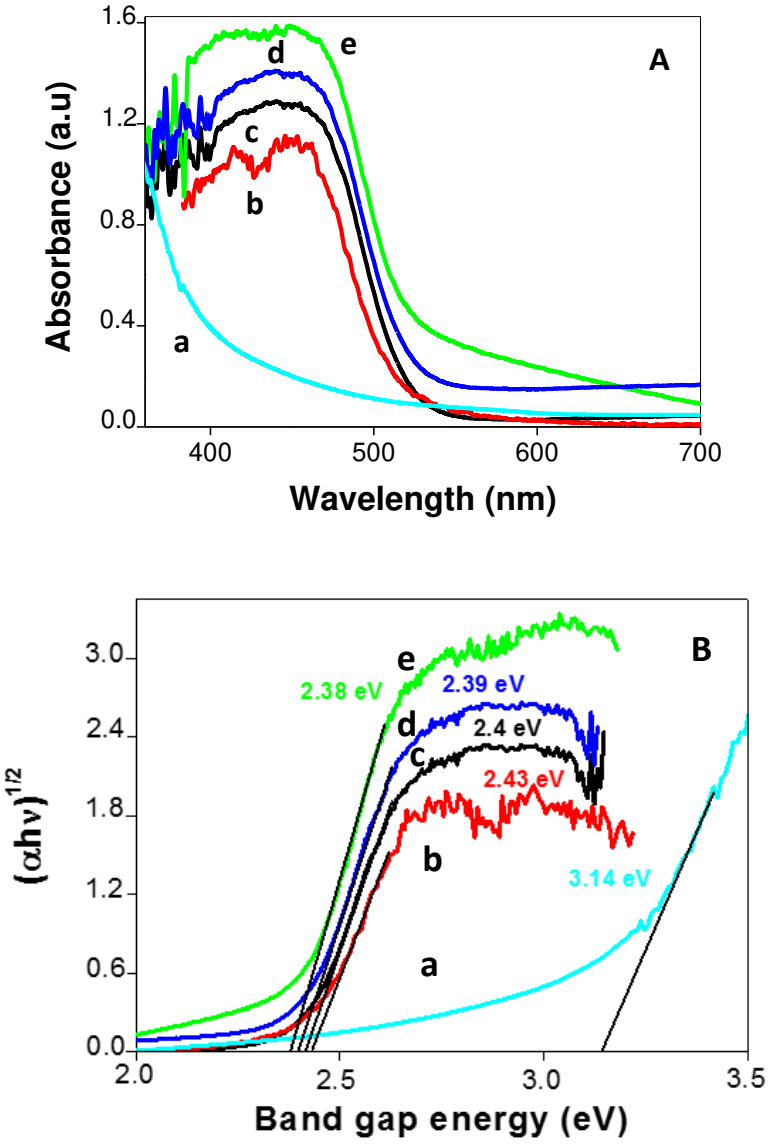

Fig. 8. (A) UV-Vis diffuse absorption spectra and (B) the plots of $(\alpha h\nu)^{1/2}$ versus photon energy ($h\nu$) of (a) pure 3DOM TiO_2, (b) 0.2$BiVO_4$/3DOM TiO_2, (c) 0.4$BiVO_4$/3DOM TiO_2 and (e) 0.6$BiVO_4$/3DOM TiO_2 nanocomposites and (e) pure $BiVO_4$ nanoparticles.

The highest photoluminescence intensity is observed for 3DOM TiO_2, indicating its high photogenerated electron–hole recombination efficiency which could lead to a reduced

photocatalytic activity. For all $BiVO_4$/3DOM TiO_2 samples (spectra b-f), the PL spectrum shows a strong emission at *525* nm which originates from the recombination of the hole formed from the hybrid orbitals of Bi 6s and O 2p (valence band VB) and the electron generated from the V 3d orbitals (conduction band CB) [47]. Compared with the inverse opal structure TiO_2, the PL emission decreases significantly for all nanocomposites. The PL intensity is progressively reduced with increasing $BiVO_4$ amount in the 3DOM TiO_2 IO structure. This behaviour shows that efficient charge or energy transfer occurs at the $BiVO_4$/TiO_2 heterojunction interface. The PL intensity is lower as the percentage of $BiVO_4$ increases from 0.04 to 0.2. In particular, the 0.2 $BiVO_4$/TiO_2 (spectrum f) shows the lowest PL intensity as compared to other samples. The emission peak at 420 nm almost disappears, indicating the inhibition of an intrinsic radiative recombination path. Accordingly, it is inferred that the recombination rate between photogenerated holes and electrons is significantly reduced in the nanocomposite. In other words, the formation of heterojunction between $BiVO_4$ and TiO_2 is helpful to improve the transfer characteristic of photogenerated carries and to enhance the photocatalytic activity. However, as can be noted in Fig. 9 (spectra d and e) the 0.4$BiVO_4$/3DOM TiO_2 and 0.6 $BiVO_4$/3DOM TiO_2 nanocomposites show a higher PL intensity compared with that of the 0.2 $BiVO_4$/3DOM TiO_2 nanocomposite, indicating a high recombination rate. After increasing the $BiVO_4$ content in the nanocomposite it becomes even more important than the 3DOM TiO_2 amount, as shown by the XRD results; the photogenerated electron-hole charge carriers are accumulated in the $BiVO_4$ sensitizer and the recombination rate increases significantly.

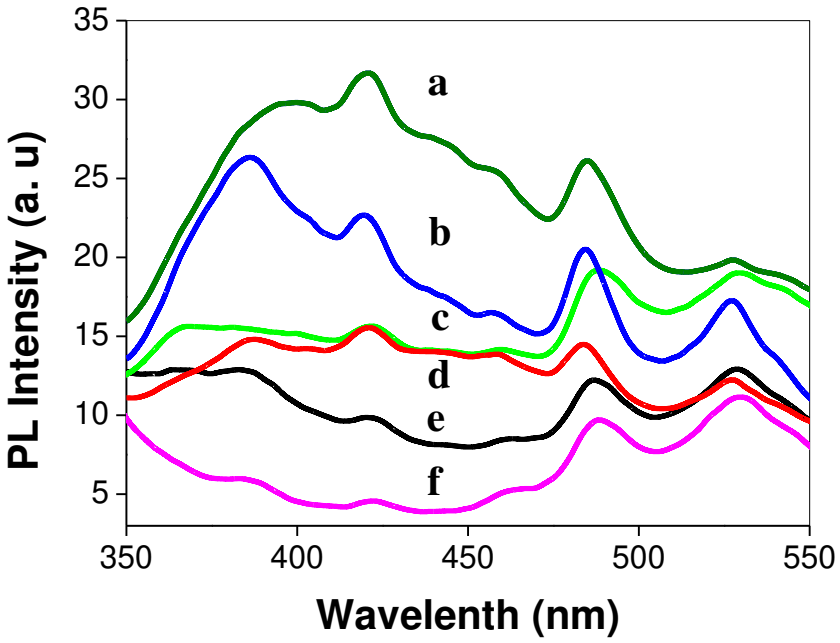

Fig. 9. Photoluminescence spectra of (a) pure 3 DOM TiO_2, (b) 0.08$BiVO_4$/3DOM TiO_2, (c) 0.04$BiVO_4$/3DOM TiO_2, (d) 0.6$BiVO_4$/3DOM TiO_2, (e) 0.4$BiVO_4$/3DOM TiO_2 and (f) 0.2$BiVO_4$/3DOM TiO_2 nanocomposites samples.

3.6 Photocatalytic performance

The photocatalytic performance of the as-prepared samples has been examined in terms of degradation of RhB in an aqueous solution under visible-light irradiation. In our previous work the 3DOM TiO_2 inverse opal structure, dumbbell-like $BiVO_4$ nanoparticles, 0.04 $BiVO_4$/3DOM TiO_2 and 0.08 $BiVO_4$/3DOM TiO_2 nanocomposite photocatalysts were studied [36]. Herein the photocatalytic activity of three new nanocomposites labeled 0.2 $BiVO_4$/3DOM TiO_2, 0.4$BiVO_4$/3DOM TiO_2 and 0.6$BiVO_4$/3DOM TiO_2 was measured under the same conditions. All results are compared, as shown in Fig. 10, in order to evaluate the variation of the photocatalytic efficiency by increasing the amount of the $BiVO_4$ nanoparticles in the nanocomposite.

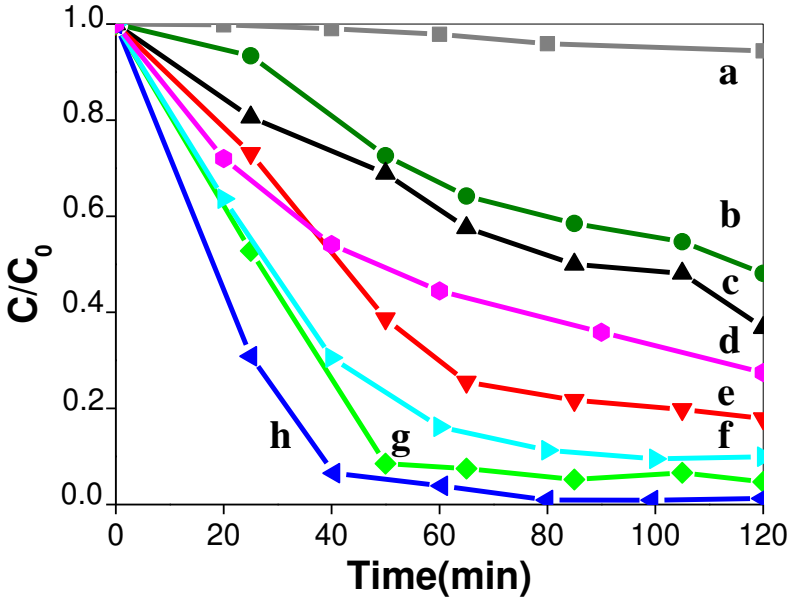

Fig. 10. Photocatalytic degradation of RhB over the as-prepared samples under visible-light irradiation: (a) Blank, (b) $BiVO_4$ nanoparticles (c) 3DOM TiO_2, (d) 0.6$BiVO_4$/3DOM TiO_2, (e) 0.04$BiVO_4$/3DOM TiO_2, (f) 0.4$BiVO_4$/3DOM TiO_2, (g) 0.08$BiVO_4$/3DOM TiO_2 and (h) 0.2$BiVO_4$/3DOM TiO_2.

A Blank experiment (curve a) in the absence of any photocatalyst shows no significant change in the RhB concentration. As can be seen the photodegradation rate for all samples increases as the reaction time increases. The dumbbell-like $BiVO_4$ (curve b) shows a very poor photocatalytic activity, only 22% of RhB being degraded in 120 min which can be related to the intrinsic properties of the $BiVO_4$ samples, such as the very poor adsorptive performance towards organic dye molecules and the inefficient migration of photogenerated electron–hole pairs to the surface for photocatalytic reactions. Thus $BiVO_4$ nanoparticles exhibit a very low activity despite its absorption in the visible light related to its narrow band gap energy of 2.4eV. TiO_2 has a large electronic band gap and it absorbs only in the UV range, however the photocatalytic performance is higher than that of $BiVO_4$ nanoparticles but it is still relatively poor, only 28% being degraded in 120 min (curve c). The reason is probably related to the 3DOM TiO_2 IO structure which can provide a more active surface area, more contact area and an increased mass transfer because of its highly accessible 3D porosity.

After the introduction of $BiVO_4$ nanoparticles, the photocatalytic activity is tremendously improved compared with the original 3DOM TiO_2 inverse opal structure and pure BiVO4

nanoparticles. The photocatalytic performance of the coupled $BiVO_4$/3DOM TiO_2 nanocomposite increases and then decreases after reaching a maximum value as the proportion of $BiVO_4$ increases from 0.04 to 0.6. The 0.2$BiVO_4$/3DOM TiO_2 (curve h) exhibits the highest photocatalytic activity, and about 100% of RhB is photodegraded in the aqueous solution after visible-light irradiation for 80 min. For the 0.04$BiVO_4$/3DOM TiO_2 (curve e), 0.08$BiVO_4$/3DOM TiO_2 (curve g), 0.4$BiVO_4$/3DOM TiO_2 (curve f) and 0.6 $BiVO_4$/3DOM TiO_2 (curve d), the conversion rate of RhB is about 80%, 95%, 90% and 85%, respectively. From the photodegradation rate of RhB, it can be inferred that the order of the photocatalytic activity is:

0.2$BiVO_4$/3DOM TiO_2 > 0.08$BiVO_4$/3DOM TiO_2 > 0.4$BiVO_4$/3DOM TiO_2 > 0.04$BiVO_4$/3DOM TiO_2 > 0.0.6$BiVO_4$/3DOM TiO_2 > 3DOM TiO_2 >$BiVO_4$

The enhanced photocatalytic activity of 0.2$BiVO_4$/3DOM TiO_2 may originate from the interfacial transfer of electrons and holes as observed by PL and XPS. The formation of a heterojunction structure between $BiVO_4$ and 3DOM TiO_2 effectively promotes the separation of photogenerated charge carriers, due to the suitable band alignment between the coupled semiconductors, and extends the absorption wavelength to the visible region. The lifetime of the charge carriers is increased and thus the recombination of electron–hole pairs can be inhibited and the photogenerated high energy can be easily transferred from the $BiOV_4$ to 3DOM TiO_2 under the internal field induced by the electronic band structure. Thus, the electrons and holes have more opportunities to participate in reduction and oxidation reactions for the degradation of the organic dye on their surface which results in an increase of the photocatalytic efficiency under visible-light irradiation. Moreover, the 3DOM inverse opal structure with interconnected pores and a high surface area could provide more active sites and more contact surface. As the amount of $BiVO_4$ nanoparticles increases, the sensitization effect increases; more electrons and holes are photogenerated and will participate in the oxidation/reduction process and an improved photocatalytic effect is found. However, the photocatalytic performance reaches a maximum for 0.2 $BiVO_4$/3DOM TiO_2; after that, it decreases with an increase of the amount of $BiVO_4$ nanoparticles in the nanocomposite. Two reasons could account for the low visible light photocatalytic activity of the 0.4 $BiVO_4$/3DOM TiO_2 and 0.6 $BiVO_4$/3DOM TiO_2 nanocomposites compared with that of 0.2 $BiVO_4$/3DOM TiO_2. First, the photogenerated electron/holes are accumulated at the surface of the $BiVO_4$ nanoparticles since the transfer of electrons to 3DOM TiO_2 is reduced due to the decreased

TiO_2 amount, the recombination rate thus increases as shown by the PL spectra. The PL intensity is more important for the 0.4 $BiVO_4$/3DOM TiO_2 and 0.6 $BiVO_4$/3DOM TiO_2, respectively, compared with that of 0.2 $BiVO_4$/3DOM TiO_2 photocatalyst, indicating their high recombination rate. Second, some of the photogenerated electrons can be transferred to TiO_2 and participate in the reduction process. However the interfacial charge process is limited by two factors: the low amount of 3DOM TiO_2 as confirmed by XRD analysis and the decrease of the surface area after increasing the amount of $BiVO_4$ nanoparticles as shown by the BET results. As known, the 3DOM photonic structure of TiO_2 with its 3D open meso-macroporosity and large surface area can facilate the diffusion and high accessibility of the dye molecules to the active sites and offer enhanced light propagation owing to multiple scattering and slow photon effect. Moreover, the inverse opal structure of TiO_2 with an open interconnected porous network facilitates the separation of the electron-hole pairs, which might generate more radical species with a strong oxidation capability for dye degradation. For the 0.4 $BiVO_4$/3DOM TiO_2 and 0.6 $BiVO_4$/3DOM TiO_2 nanocomposites, as the amounts of 3DOM TiO_2 decrease compared with $BiVO_4$ nanoparticles the surface area decreases significantly. The adsorptive performance of $BiVO_4$/3DOM TiO_2 nanocomposites become very poor and the dye molecules diffusion is reduced. These factors are unfavorable for photocatalysis.

A pseudo-first-order kinetic model was employed to fit the degradation data by using the linear transformation: $\ln(C_0/C_t) = kt$ (k is the kinetic constant, while C_0 and C_t are the initial concentration and the concentration of RhB during the reaction time, respectively). The kinetics of RhB degradation over the $BiVO_4$/3DOM TiO_2 nanocomposites with different composition, pure 3DOM TiO_2 inverse opal structure and $BiVO_4$ nanoparticles are presented in Fig. 11. The kinetic constants of the pure $BiVO_4$ nanoparticles, pure 3DOM TiO_2, 0.04$BiVO_4$/3DOM TiO_2, 0.08$BiVO_4$/3DOM TiO_2, 0.2$BiVO_4$/3DOM TiO_2, 0.4$BiVO_4$/3DOM TiO_2 and 0.6$BiVO_4$/3DOM TiO_2 nanocomposites photocatalysts are 0.0062, 0.0078, 0.0152, 0.0256, 0.0381, 0.0209 and 0.0110, respectively, as represented by the histogram in Fig. 12.

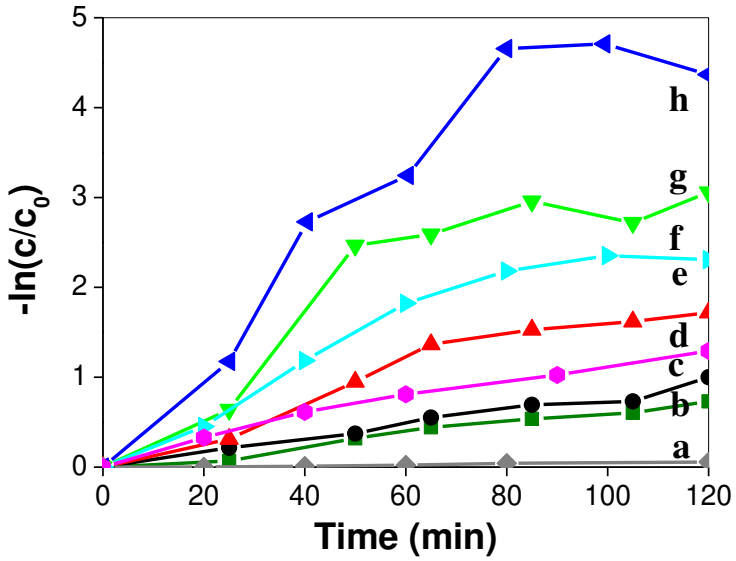

Fig. 11. Kinetic curves of RhB photocatalytic degradation over different samples: (a) Blank, (b) $BiVO_4$ nanoparticles (c) 3DOM TiO_2, (d) 0.6$BiVO_4$/3DOM TiO_2, (e) 0.04$BiVO_4$/3DOM TiO_2, (f) 0.4$BiVO_4$/3DOM TiO_2, (g) 0.08$BiVO_4$/3DOM TiO_2 and (h) 0.2$BiVO_4$/3DOM TiO_2.

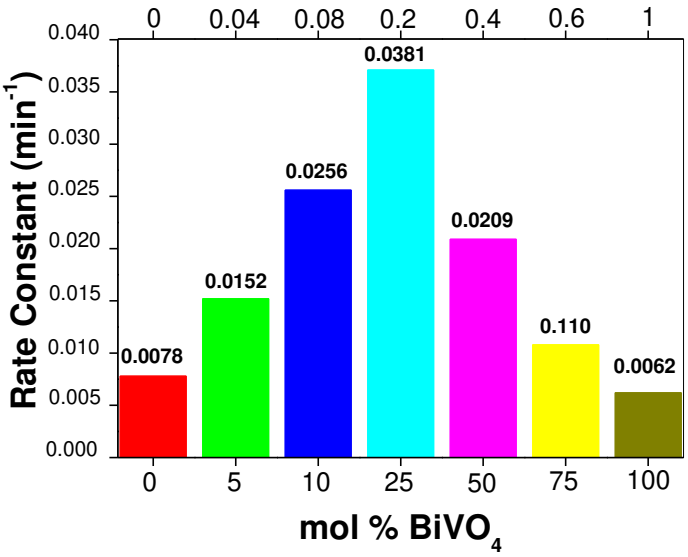

Fig. 12. Variation of the reaction constant with different molar ratios.

As can be seen, the photocatalytic efficiency of the $BiVO_4$/3DOM TiO_2 nanocomposites increases significantly with the amount of $BiVO_4$ nanoparticles to reach a maximum for 0.2 $BiVO_4$/3DOM TiO_2. As we explained in the discussion above, the enhanced photocatalytic activity of the 0.2$BiVO_4$/3DOM TiO_2 nanocomposite is attributed to the synergy of the

structural effect in which 3DOM structures with an open interconnected porous network facilitate the diffusion of molecules and offer a larger surface area and the formation of $BiVO_4/TiO_2$ heterojunctions. This effect is favorable for photocatalysis and the interfacial charge transfer, which may lead to an even higher quantum efficiency, supplying more photogenerated electrons in photocatalytic reactions. Moreover, $BiVO_4$ nanoparticles act as light sensitizer leading to visible light absorbing materials and more electron and hole charge carriers are photogenerated. The schematic representation of energy band diagram and charge transfer process in $BiVO_4$/3DOM TiO_2 nanocomposites are given in Fig. 13. When the $BiVO_4$/3DOM TiO_2 nanocomposite photocatalyst is irradiated using visible light (> 400 nm), electrons in the valence band (VB) of the $BiVO_4$ nanoparticles are excited to the conduction band (CB), creating holes in the VB. Because the CB edge potential of $BiVO_4$ is more negative than that of TiO_2, the photogenerated electrons of $BiVO_4$ tend to migrate to the CB of TiO_2. The photogenerated holes, which have oxidizing power, are more favorable to react with adsorbed H_2O to produce reactive $\cdot OH$ radicals. The photogenerated electrons are good reductants, which can be captured by the adsorbed O_2 molecules at the surface of the catalyst and reduce them to $O^{\cdot-}_2$ radicals. These radicals are the main active species to react with the RhB molecules adsorbed at the surface of the nanocomposite during the degradation process. Therefore, the charge transfer between the coupled semiconductors is very beneficial for promoting the photocatalytic activity. The formation of heterojunctions affects the charge separation properties of the composite photocatalyst; the different band gap positions of $BiVO_4$ and TiO_2 allow the visible light photogenerated electrons to flow from the CB of $BiVO_4$ into the CB of TiO_2 so that the recombination of electron-hole (e-h) pairs is suppressed and thus the quantum efficiency is enhanced. As a result, a higher photocatalytic oxidation activity is achieved for the $BiVO_4$/3DOM TiO_2 composite. However, when the proportion of $BiVO_4$ in nanocomposites is higher than 25 mol%, the photogenerated electrons will remain at the surface of $BiVO_4$ and can not be efficiently transferred to TiO_2 as indicated in Fig. 13 due to too low amount of TiO_2 in nanocomposites, leading to high recombination rate of electrons-holes and the highly reduced photocatalytic activity. The amount of $BiVO_4$ as highly efficient visible light sensitizer should be carefully controlled to develop a highly active photocatalyst for dye pollutants degradation.

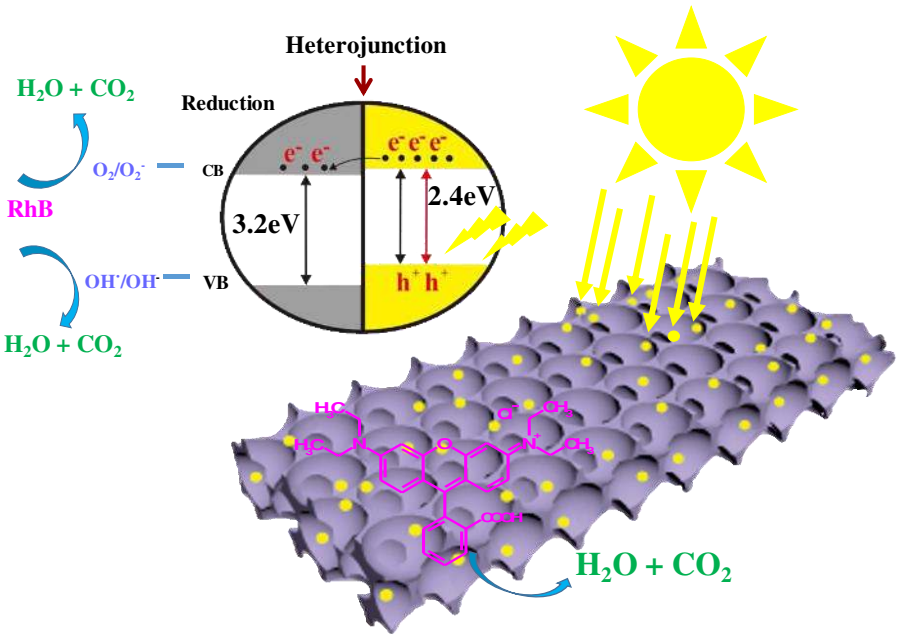

Fig. 13. Schematic representation of energy band diagram and charge transfer process in the $BiVO_4$@3DOM TiO_2 nanocomposite.

Conclusion

The introduction of $BiVO_4$ nanoparticles was found to extend the spectral response of TiO_2 from the UV to the visible region and to enhance significantly the photocatalytic efficiency towards the degradation of RhB under visible-light irradiation. $BiVO_4$ nanoparticles in the 3DOM TiO_2 inverse opal structure act as a very significant sensitizer to absorb visible light and to transfer efficiently high energy electrons to TiO_2. The formation of heterojunction between $BiVO_4$ and 3DOM TiO_2 induces a more efficient separation of excess charge carriers and retards the recombination of charge pairs, thereby facilitating the interparticle electron transfer at the $BiVO_4$/3DOM TiO_2 interfaces. The phtotcatalytic activity depends on the amount of $BiVO_4$ in nanocomposites. The photocatalytic performance increases to reach a maximum for the 0.2 $BiVO_4$/3DOM TiO_2. From this value on, as the $BiVO_4$ content increases, the reaction rate decreases. This behavior can be attributed to: 1) the photogenerated electron/holes which are accumulated at the surface of the $BiVO_4$ nanoparticles, leading to easy recombination of photogenerated electron/holes as the $BiVO_4$ amount increases, 2) the low amount of 3DOM TiO_2 resulting in the reduction of surface area of nanocomposites and 3) the poor adsorptive properties of the $BiVO_4$ nanoparticles.

Acknowledgements

This work was realized with the financial support of Chinese Ministry of Education in a framework of the Changjiang Scholar Innovative Research Team Program (IRT_15R52). B. L. Su acknowledges the Chinese Central Government for an “Expert of the State” position in the Program of the “Thousand Talents” and a Clare Hall Life Member, University of Cambridge. Y. Li acknowledges Hubei Provincial Department of Education for the “Chutian Scholar” program. This work is also supported by PhD Programs Foundation (20120143120019) of Chinese Ministry of Education, the Wuhan Youth Chenguang Program of Science and Technology (2013070104010003), Hubei Provincial Natural Science Foundation (2014CFB160, 2015CFB516), the National Science Foundation for Young Scholars of China (No. 51502225) and Self-determined and Innovative Research Funds of the SKLWUT (2015-ZD-7). Z. Y. Hu and G. Van Tendeloo acknowledge support from the EC Framework 7 program ESTEEM2 (Reference 312483). This research used resources of the Electron Microscopy Service located at the University of Namur. This Service is member of the “Plateforme Technologique Morphologie - Imagerie”. The XPS analyses were made in the LISE, Department of Physics of University of Namur thanks to Dr. P. Louette. XRD measurements, UV-visible and photoluminescent spectroscopic analyses and N_2 adsorption-desorption measurements were made with the facility of the “Plateforme Technologique Physico-Chimique”.

References

[1] Q. Liu, J. He, T. Yao, Z. Sun, W. Cheng, S. He, Y. Xie, Y. Peng, H. Cheng and Y. Sun, *Nat. Commun.,* 2014, 5.

[2] H. Li, Y. Zhou, W. Tu, J. Ye and Z. Zou, *Adv. Funct. Mater.,* 2015, 25, 998-1013.

[3] Q. Li, X. Li, S. Wageh, A. Al-Ghamdi and J. Yu, *Adv. Ener. Mater.,* 2015, 5.

[4] H. Tong, S. Ouyang, Y. Bi, N. Umezawa, M. Oshikiri and J. Ye, *Adv. Mater*., 2012, 24, 229-251.

[5] Y. W. Cheng, R. C. Y. Chan and P. K. Wong, *Water Res*., 2007, 41, 842-852.

[6] J. H. Park, S. Kim and A. J. Bard, *Nano. Lett*., 2006, 6, 24-28.

[7] M. Ksibi, S. Rossignol, J.M. Tatibouët and C. Trapalis, *Mater. Lett*., 2008, 62, 4204-4206.

[8] L. G. Devi, N. Kottam and S. G. Kumar, *J. Phys. Chem. C*, 2009, 113, 15593-15601.

[9] H. Cheng, B. Huang and Y. Dai, *Nanoscale,* 2014, 6, 2009-2026.

[10] Y. Huang, B. Long, H. Li, M.S. Balogun, Z. Rui, Y. Tong and H. Ji, *Adv. Mater. Interfaces*, 2015, 2.

[11] M. Guan, C. Xiao, J. Zhang, S. Fan, R. An, Q. Cheng, J. Xie, M. Zhou, B. Ye and Y. Xie, *J. Am. Chem. Soc.,* 2013, 135, 10411-10417.

[12] Y. Ma, Y. Jia, Z. Jiao, M. Yang, Y. Qi and Y. Bi, *Chem. Commun.,* 2015, 51, 6655-6658.

[13] X. Chang, T. Wang, P. Zhang, J. Zhang, A. Li and J. Gong, *J. Am. Chem. Soc.,* 2015, 137,
8356-8359.

[14] L. Ye, J. Liu, C. Gong, L. Tian, T. Peng and L. Zan, *ACS Catal.,* 2012, 2, 1677-1683.

[15] G. Liu, T. Wang, S. Ouyang, L. Liu, H. Jiang, Q. Yu, T. Kako and J. Ye, *J. Mater. Chem. A*, 2015, 3, 8123-8132.

[16] A. Kudo, K. Ueda, H. Kato and I. Mikami, Catal. Lett., 1998, 53, 229-230.

[17] A. Kudo, K. Omori and H. Kato, J. Am. Chem. Soc., 1999, 121, 1459-11467.

[18] S. Kohtani, M. Koshiko, A. Kudo, K. Tokumura, Y. Ishigak A. Toriba, K. Hayakawa, R. Nakagaki, Appl. Catal. B, 2003, 46, 573-586.

[19] S. Kohtani, J. Hiro, N. Yamamoto, A. Kudo, K. Tokumura and R. Nakagaki, Catal. Commun., 2005, 6, 185-189.

[20] K. Sayama, A. Nomura, Z. Zou, R. Abe, Y. Abe and H. Arakawa, Chem. Commun., 2003, 9, 2908-2909.

[21] X. Zhang, Z. Ai, F. Jia, L. Zhang, X. Fan and Z. Zou, Mater. Chem. Phys., 2007, 103, 162-167.

[22] H. T. Yu, X. Quan, S. Chen and H.M. Zhao, *J. Phys. Chem. C,* 2007, 111, 12987.
[23] H. Zhang, X. J. Lv , Y. M. Li , Y. Wang and J.H. Li , *ACS Nano.,* 2010, 4, 380 .
[24] H. Huang, S. Wang, Y. Zhang, P.K. Chu, *RSC Adv.,* 2014, 4, 41219 .
[25] S. B. Rawal , S. Bera , D. Lee , D. J. Jang and W.I. Lee , *Catal. Sci. Technol.,* 2013, 3, 1822.
[26] S. Obregon, S. W. Lee and G. Colon, *Dalton Trans*., 2014, 43, 311–316.
[27] B. Cao, J. Peng and Y. Y., *J. Cluster Sci*., 2013, 24, 771–785.
[28] L. Zhang, G. Tan, S. Wei, H. Ren, A. Xia and Y. Luo, *Ceram. Int*., 2013, 39, 8597–8604.
[29] Y. Hu, D. Li, Y. Zheng, W. Chen, Y. He, Y. Shao, X. Fu and G. Xiao, *Appl. Catal., B*, 2011, 104, 30–36.
[30] G. Long, F. Fresno, S. Grosss and U. L. Stangar, Environ. Sci. Pollut. *Res. Int*., 2014, 21, 11189–11197.
[31] R. Rahimi, S. Zargari and M. M. Moghaddas, *Adv. Mater. Res*., 2013, 702, 172–175.
[32] M. Xie, X. Fu, L. Jing, P. Luan, Y. Feng and H. Fu, *Adv. Energy Mater*., 2014, 4, 130095.
[33] S. Ho-Kimur, S. J. A. Moniz, A. D. Handoko and J. W. Tang, *J. Mater. Chem. A*, 2014, 2, 3948–3953.
[34] H. Li, H. Yu, X. Quan , S. Chen and H. Zhao, *Adv. Funct. Mater*., 2015, 25, 3074–3080
[35] X. Zhu, F. Zhang, M. Wang, X. Gao, Y. Luo, J. Xue, Y. Zhang, J. Ding, S. Sun and C. Gao, *Appl. Catal. A*, 2015, 15, 30194.
[36] M. Zalfani, B. Van Der Schueren, Z.Y. Hu, J. Rooke, R. Bourguiga, M. Wu, G. Van Tendeloo, Y. Li and B.L. Su, *J. Mater. Chem. A*, 2015, 3, 21244–21256.
[37] M. Zalfani, B. van der Schueren, M. Mahdouani, R. Bourguiga, W. B. Yu, M. Wu, O. Deparis, Y. Li and B. L. Su, *Appl. Catal. B*, 2016, 187-198
[38] M. Wu, J. Liu, J. Jin, C. Wang, S. Z. Huang, Z. Deng, Y. Li and B. L. Su, *Appl. Catal. B*, 2014, 150-151, 411-420
[39] M. Wu, J. Jin, J. Liu, O. Deparis and B. L. Su, *J. Mater. Chem. A*, 2013, 1, 15491-15500
[40] M. Wu, A. Zheng, F. Deng and B. L. Su, *Appl. Catal. B*, 2013, 138-139, 219-228
[41] M. Wu, Y. Li, Z. Deng, B. L. Su, *ChemSusChem*, 2011, 4, 1481-1488
[42] S.D. Richardson, C.S. Wilson, K.A. Rusch, *Ground Water*, 2004, 42, 678.
[43] D. Kornbrust, T. Barfknecht, *Environ. Mutagen.,* 1985, 7 101.
[44] D.B. McGregor, A.G. Brown, S. Howgate, D. McBride, C. Riach, W.J. Caspary, *Environ. Mol. Mutagen.*,199, 17, 196.

[45] Q. Wang, C.C. Chen, D. Zhao, W.H. Ma, J.C. Zhao, *Langmuir*, 2008, 24, 7338.

[46] F. Chen, J.C. Zhao, H. Hidaka, *Int. J. Photoenergy,* 2003, 5, 209.

[47] X.F. Hu, T. Mohamood, W.H. Ma, C.C. Chen, J.C. Zhao, *J. Phys. Chem. B*, 2006, 110, 26012.

[48] S.K. Kansal, M. Singh, D. Sud, *J. Hazard. Mater.*, 2007, 141, 581–590.

[49] K. Yu, S. Yang, H. He, C. Sun, C. Gu, Y. Ju, *J. Phys. Chem. A*, 2009, 113, 10024–10032.

[50] M. Sun, D. Li, Y. Chen, W. Chen, W. Li, Y. He, X. Fu, *J. Phys. Chem. C*, 2009, 113, 13825–13831.

[51] Z. He, C. Sun, S. Yang, Y. Ding, H. He, Z. Wang, *J. Hazard. Mater.*, 2009, 162, 1477–1486.

[52] J. Luan, M. Li, K. Ma, Y. Li, Z. Zou, *Chem. Eng. J.*, 2011, 167, 62–171.

[53] A. Mehrdad, B. Massoumi, R. Hashemzadeh, *Chem. Eng. J.*, 2011, 168, 1073–1078.

[54] Y. Huang, H. Li, M. S. Balogun, W. Liu, Y. Tong, X. Lu and H. Ji, *ACS Appl. Mater. Interfaces,* 2014, 6, 22920-22927.

[55] L. Chen, Q. Zhang, R. Huang, S. F. Yin, S. L. Luo and C. T. Au, *Dalton Trans*., 2012, 41, 9513-9518.

[56] C.J. Li, P. Zhang, R. Lv , J.W. Lu , T. Wang , S.P. Wang , H.F. Wang and J.L. Gong , *Small,* 2013, *9*, 3951 .

[57] X. Xue, W. Ji, Z. Mao, H. Mao, Y. Wang, X. Wang, W. Ruan, B. Zhao and J.R. Lombardi, *J. Phys. Chem. C*, 2012, 116, 8792-8797.

[58] C. Kim, K.S. Kim, H.Y. Kim and Y.S. Han, *J. Mater. Chem*., 2008, 18, 5809-5814.

[59] M. Shang, W. Wang, L. Zhou, S. Sun, W. Yin, *J. Hazard. Mater*., 2009, 172, 338.

[60] B. Cheng, W. Wang, L. Shi, J. Zhang, J. Ran and H. Yu, *Int. J. Photoenergy*, 2012, 1.

[61] Z. Xiong, L. L. Zhang, J. Ma and X. S. Zhao, *Chem. Commun*., 2010, 46, 6011–6099.

[62] J. Su, L. Guo, N. Bao and C. A. Grimes*, Nano Lett.*, 2011, 11, 1928–1933.

[63] Y. Fu, X. Sun and X. Wang, *Mater. Chem. Phys*., 2011, 131, 325.

*Graphical Abstract

Graphical Abstract

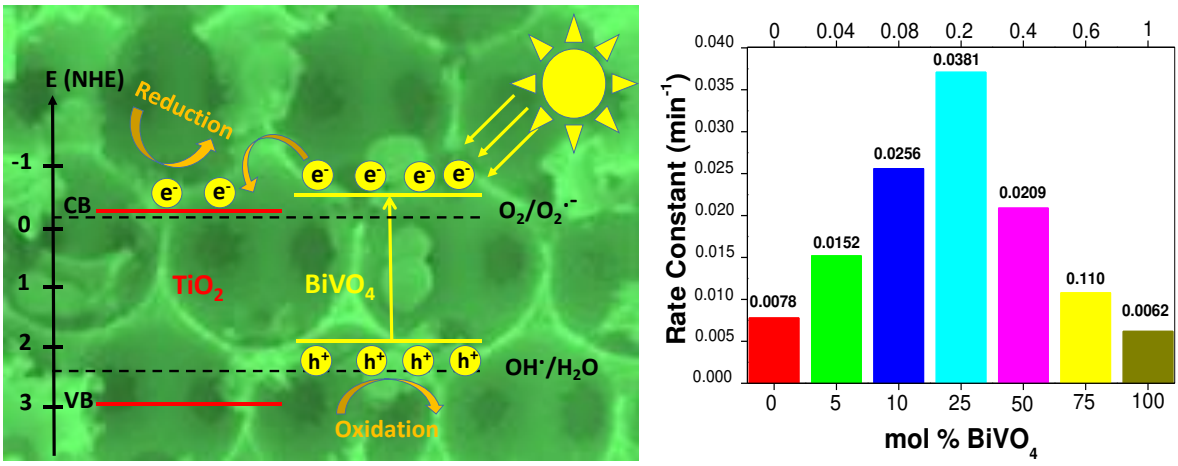

The effect of the amount of $BiVO_4$ as visible light sensitizer on the photocatalytic activity of $BiVO_4$/3DOM TiO_2 nanocomposites was highlighted. The low amount of $BiVO_4$ nanoparticles favors the transfer of photogenerated electrons to 3DOM TiO_2 while photogenerated electrons will remain at the surface of $BiVO_4$ at high amount of $BiVO_4$, leading to the recombination of electrons-holes and reduced photocatalytic activity.